

ing in a bending of the AFM cantilever and an increase in the shear stress at the interface. The cantilever bending increased until the force applied to the nanotube was sufficient to pull the nanotube from the polymer (Fig. 1) owing to interfacial failure in shear. This test was repeated using larger nanotube embedded lengths by pushing the nanotube at different depths into the liquid. The embedded lengths were evaluated from SEM images of the nanotube before and during embedment within the epoxy. Further experiments were performed using carbon nanotubes that had been previously chemically modified with carboxylic groups [12] to improve the adhesion with the epoxy matrix.

Received: May 20, 2005

Final version: July 6, 2005

Published online: December 5, 2005

DOI: 10.1002/adma.200500508

Field Emission of Electrons from Single LaB₆ Nanowires**

By Han Zhang, Jie Tang, Qi Zhang, Gongpu Zhao, Guang Yang, Jian Zhang, Otto Zhou, and Lu-Chang Qin*

Lanthanum hexaboride (LaB₆) single crystals have been one of the most widely used thermionic electron sources in a large variety of devices requiring electron emission. The low work function (~2.6 eV)^[1] together with low vapor pressure at high temperature^[2] makes LaB₆ a thermionic electron cathode material superior to conventional filamentous tungsten in electron optical instruments such as the transmission electron microscope and the scanning electron microscope. To pursue higher performance in these microscopy applications, field-emission (FE) electron sources have been introduced to achieve an even higher brightness and lower energy spread. W or W/ZrO based field-emission guns (FEG) are now commercially available and can offer a brightness two orders of magnitude higher than the LaB₆ thermionic electron gun.^[3] The brightness of an FEG is proportional to the current density J of electrons emitted from the cathode surface, which can be described by the zero-temperature Fowler–Nordheim (F–N) equation (in A cm⁻²) as^[4]

$$J = 1.5 \times 10^{-6} \frac{E^2}{\phi} \exp\left(\frac{10.4}{\phi^{1/2}} - \frac{6.44 \times 10^7 \phi^{3/2}}{E}\right) \quad (1)$$

where ϕ is the cathode material's work function and E is the local electric field applied on the cathode tip, which can be expressed as $E = V/5r$ with V being the applied voltage and r the radius of the cathode tip.

The above relations show that a lower work function and a smaller tip radius of the cathode result in a higher emission current density. Stimulated by the fact that LaB₆ has a much lower work function than W or W/ZrO and that it offers ex-

- [1] M-F. Yu, O. Lourie, M. J. Dyer, K. Moloni, T. F. Kelly, R. S. Ruoff, *Science* **2000**, 287, 637.
- [2] M-F. Yu, B. S. Files, S. Arepalli, R. S. Ruoff, *Phys. Rev. Lett.* **2000**, 84, 5552.
- [3] B. G. Demczyk, Y. M. Wang, J. Cumings, M. Hetman, W. Han, A. Zettl, R. O. Ritchie, *Mater. Sci. Eng. A* **2002**, 334, 173.
- [4] M. M. J. Treacy, T. W. Ebbesen, J. M. Gibson, *Nature* **1996**, 381, 678.
- [5] A. Krishnan, E. Dujardin, T. W. Ebbesen, P. N. Yianilos, M. M. J. Treacy, *Phys. Rev. B* **1998**, 58, 14013.
- [6] W. Wong, P. E. Sheehan, C. M. Lieber, *Science* **1997**, 277, 1971.
- [7] C. A. Cooper, S. R. Cohen, A. H. Barber, H. D. Wagner, *Appl. Phys. Lett.* **2002**, 81, 3873.
- [8] A. H. Barber, S. R. Cohen, H. D. Wagner, *Appl. Phys. Lett.* **2003**, 82, 4140.
- [9] A. H. Barber, S. R. Cohen, S. Kenig, H. D. Wagner, *Compos. Sci. Tech.* **2004**, 64, 2283.
- [10] R. Z. Li, L. Ye, Y. W. Mai, *Compos. A* **1997**, 28, 73.
- [11] J. Chen, M. A. Hamon, H. Hu, Y. S. Chen, A. M. Rao, P. C. Eklund, R. C. Haddon, *Science* **1998**, 282, 95.
- [12] A. Eitan, K. Jiang, D. Dukes, R. Andrews, L. S. Schadler, *Chem. Mater.* **2003**, 15, 3198.
- [13] A. Bukuwska, W. Bukowski, *Org. Process Res. Devel.* **1990**, 3, 432.
- [14] L. Shechter, J. Wynstra, *Industr. Eng. Chem.* **1956**, 48, 86.
- [15] J. Cumming, A. Zettl, *Science* **2000**, 289, 602.
- [16] A. Kelly, W. R. Tyson, *J. Mech. Phys. Solids* **1965**, 13, 329.
- [17] H. L. Cox, *Brit. J. Appl. Phys.* **1952**, 3, 72.
- [18] S. J. V. Frankland, A. Caglar, D. W. Brenner, M. Griebel, *J. Phys. Chem. B* **2002**, 106, 3046.
- [19] L. Liu, A. H. Barber, S. Nuriel, H. D. Wagner, *Adv. Funct. Mater.* **2005**, 15, 975.
- [20] Z.-F. Li, D. T. Grubb, *J. Mater. Sci.* **1994**, 29, 189.
- [21] H. Nishijima, S. Kamo, S. Akita, Y. Nakayama, K. I. Hohmura, S. H. Yoshimura, K. Takeyasu, *Appl. Phys. Lett.* **1999**, 74, 4061.
- [22] A. H. Barber, S. R. Cohen, H. D. Wagner, *Phys. Rev. Lett.* **2004**, 92, 186103.
- [23] J. E. Sader, J. W. M. Chon, P. Mulvaney, *Rev. Sci. Instr.* **1999**, 70, 3967.

[*] Prof. L.-C. Qin, H. Zhang, Prof. O. Zhou
Curriculum in Applied and Materials Sciences
University of North Carolina at Chapel Hill
Chapel Hill, NC 27599-3255 (USA)
E-mail: lcqin@physics.unc.edu

Prof. L.-C. Qin, Dr. J. Tang, Dr. Q. Zhang, G. Zhao, G. Yang,
Dr. J. Zhang, Prof. O. Zhou
Department of Physics and Astronomy
University of North Carolina at Chapel Hill
Chapel Hill, NC 27599-3255 (USA)
Dr. J. Tang
National Institute for Materials Science
Tsukuba, Ibaraki 305-0047 (Japan)

[**] We thank Dr. Minghui Song for EELS analysis and the W. M. Keck Foundation for financial support. J. Tang is partially supported by the Japan–US Collaborative Scientific Program.

cellent performance as a thermionic electron source, extensive field-emission studies have been carried out on electro-etched LaB₆ needles with tip radii ranging from 100 nm to 300 nm in the search of a brighter field-emission electron source.^[5-9] High temperature field-emission studies showed that a brightness at least two orders of magnitude higher than that of a LaB₆ thermionic emitter could be achieved with good stability and that only half of the local electric field was necessary to draw substantial current from the LaB₆ needles compared to a thermal-assisted W/ZrO FEG, which was attributed to the lower work function of LaB₆. However, when the electron emission is operated at high temperature, it requires a higher vacuum and has a larger energy spread in the electron beam, resulting in a larger chromatic aberration in electron coherence. In cold field-emission studies, a high-temperature flashing procedure and a high vacuum of at least 10⁻⁹ torr (1 torr ~ 133 Pa) were required throughout the measurement in order to obtain field emission. These limitations have made FE electron source applications impractical for this type of electro-etched LaB₆ needles.

One-dimensional nanotube/nanowires have very sharp tips with diameters ranging from more than a hundred to just a few nanometers. Their properties in field emission were first demonstrated in carbon nanotubes.^[10-12] The nanometer-scale tip geometry of carbon nanotubes greatly enhances the local electric field and allows stable field emission of high current density under much more practical experimental conditions, such as low applied voltage, low vacuum, and room temperature, and even without the need for the flashing procedure. These attractive features have aroused a tremendous amount of scientific interest in this field, and today its advantage over conventional field-emission electron sources has been well demonstrated.^[13-15] In the meantime, nanowires of many other materials have also been reported to show low turn-on voltage field-emission phenomena which are believed to originate from their small tip dimensions.^[16-20] However, the large work functions of these materials, including carbon nanotubes, still require tough working conditions for the utilization of these materials. To find a high-performance nanowire/nanotube field-emission cathode material, LaB₆ nanowires, which have a low work function and good electrical conductance, offer a better possibility that has not been well explored. Among all the crystal lattice planes of LaB₆, the {001} planes have both low work function and low volatility, and therefore they are usually preferred as the emission planes for commercialized LaB₆ thermionic electron guns.^[1,2] In this article, we report the synthesis by chemical vapor deposition (CVD) of <001> oriented single-crystalline LaB₆ nanowires and the measurement of their excellent FE characteristics.

Figure 1 is a typical scanning electron microscopy (SEM) image of the synthesized LaB₆ nanowires on a silicon substrate. The nanowires have lateral dimensions from a few tens of nanometers to more than 100 nm, and lengths extending to more than a few micrometers. Nanometer- and micrometer-sized cubes and rectangular platelets were also found to have grown on the substrate along with the nanowires, whose ge-

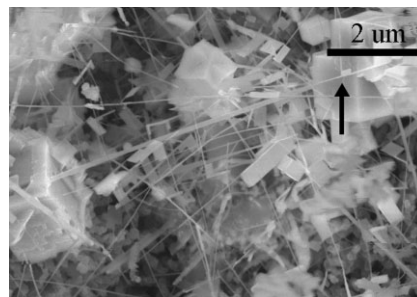


Figure 1. SEM image of single-crystalline LaB₆ nanowires synthesized on silicon substrate. Some cubes and platelets are also grown along with the nanowires. The arrow indicates a cube grown on a nanowire.

ometries reveal the crystallographic symmetries of cubic LaB₆ single crystals. These cubes and platelets sometimes form a right angle connecting two nanowires, as indicated by the arrow in Figure 1.

A typical low-magnification transmission electron microscopy (TEM) image of the produced LaB₆ nanowires is shown in Figure 2a. The nanowires are about 40 nm in lateral dimensions and more than several micrometers in length. The nanowires have smooth surfaces and their tips, indicated by the arrows in the image, are always terminated with a flat surface

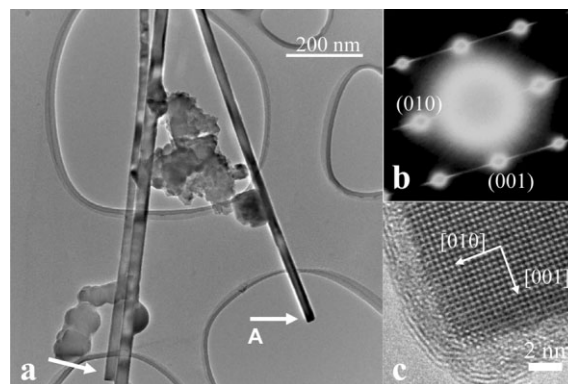


Figure 2. a) Low-magnification TEM image of LaB₆ nanowires. Arrows point to the tips terminated with a flat surface. b) Electron-diffraction pattern of the LaB₆ nanowire displayed in (a) labeled A showing [001] zone axis geometry. Streaks are perpendicular to the axial direction of the nanowire. c) High-resolution image showing the tip of the same LaB₆ nanowire, revealing the flat tip surface (001).

and form right angles with their side surfaces. Selected-area electron diffraction (SAED) was used to determine the lattice structure of the nanowires. An electron diffraction pattern of the nanowire labeled A in Figure 2a is shown in Figure 2b, showing that this nanowire was grown in the [001] crystallographic direction of the cubic LaB₆ with lattice constant $a = 4.153 \text{ \AA}$. It was also noticed that all the diffraction spots are elongated into streaks perpendicular to the [001] lattice direction, indicating that the nanowire axis is parallel to the [001] direction of the LaB₆ crystal. The diffraction pattern ap-

peared identical as we moved the SAED aperture along the entire nanowire, suggesting that the LaB₆ nanowire is single crystalline. To elucidate more details of the atomic structure of the LaB₆ nanowires, high-resolution transmission electron microscopy (HRTEM) was also employed, as shown in Figure 2c. The atomic-resolution image confirms that the nanowire is parallel to the [001] crystallographic direction of the LaB₆ crystal and also reveals that a right angle was formed between the side surfaces and the tip, even at the atomic scale. It should also be pointed out that the HRTEM image contrast near the edge of the nanowire is uniform, unlike the diminishing image contrast observed in cylindrical nanowires, suggesting that the cross-section of the LaB₆ nanowire were more likely to be square, which was also observed in the case of LaB₆ micrometer-sized whiskers,^[21,22] as well as CeB₆ and GdB₆ nanowires of the same type of crystal structure.^[23,24] To determine the chemical composition of the amorphous layer covering the nanowire, a small electron-beam probe was focused on the amorphous layer and electron energy-loss spectra (EELS) were acquired. The fact that only boron and lanthanum elements were detected suggests that the layer is composed of amorphous boron, since it is the only feasible amorphous phase among the combinations of the two elements, and the lanthanum signals were due to the electron scattering from the crystalline part of the nanowire.

LaB₆ nanowires with lateral dimensions below 20 nm were also fabricated. Figure 3 shows an HRTEM image of a LaB₆ nanowire about 15 nm in width. The growth direction of the nanowire is also parallel to its <001> lattice direction, and its surfaces are all terminated with {001} lattice planes. This thin

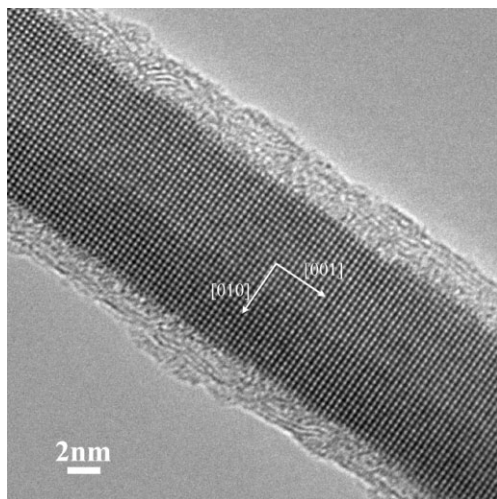


Figure 3. High-resolution TEM image of a thin LaB₆ nanowire 15 nm in width. The nanowire is single crystalline and has grown in the [001] direction.

LaB₆ nanowire is also single crystalline. The <001> growth of these LaB₆ nanowires is attributed to the fact that the {001} lattice planes of LaB₆ have the highest atomic density, and therefore, it would minimize the total energy for the crystal to

grow in this lattice direction. However, the causes of the thickness and length variations among the nanowires are still unknown, and a detailed growth mechanism still needs further investigation.

Figure 4a shows a TEM image of a single LaB₆ nanowire of 140 nm in width and about 1 μm in length attached to the tip of a 0.5 mm thick tungsten wire. Field-emission measurements of this structure were performed at a pressure of 10⁻⁷ torr in-

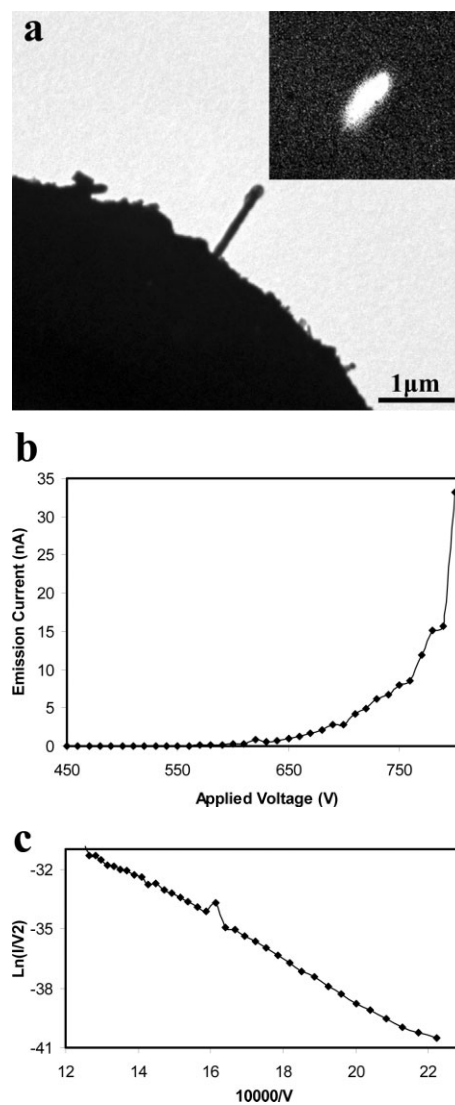


Figure 4. a) Low-magnification TEM image of a single LaB₆ nanowire field-electron emitter. Inset: Fluorescent electron emission image of the emitter recorded on the phosphor viewing screen. b) Current-voltage (*I*-*V*) curve of the field emission from the single LaB₆ nanowire emitter. c) F-N plot of $\ln(I/V^2)$ vs. $1/V$. Excellent agreement with the F-N theory of field emission is observed.

side a high-vacuum chamber. While an increasing voltage was applied, the electron fluorescent pattern observed on a phosphor screen was recorded by a charge-coupled device (CCD) camera. An observable, bright emission pattern started to ap-

pear on the phosphor screen when the applied voltage reached 650 V, and the emission pattern is shown in the inset of Figure 4a. The elliptical shape of the emission pattern is likely due to the fact that the emitter was not well aligned with respect to the applied electric field, therefore causing the cylindrical electron beam to intercept the phosphor screen at an acute angle. The emission current–voltage (I – V) curve is displayed in Figure 4b. A measurable field-emission current of 0.5 pA was obtained at 450 V, which corresponds to an average electric field of $1.5 \text{ V } \mu\text{m}^{-1}$, obtained by dividing the applied voltage by the cathode–anode separation of about 300 μm . Figure 4c shows the F–N plot, $\ln(I/V^2)$ vs. $1/V$. The good linearity of the plot suggests that the field emission from the LaB₆ nanowire emitter agrees with a metal–vacuum field-emission model as described by the F–N equation. In addition, by knowing the work function of the LaB₆ emitter (2.6 eV for the {001} planes^[1]), the slope k of the F–N plot, where $k = -6.44 \times 10^7 \phi^{3/2}/\beta$, can be used to estimate the lateral dimensions of the emitter with an enhancement factor $\beta \approx 1/5r$. For this structure, we obtained $D = 2r \approx 152 \text{ nm}$. This value falls between the edge length and the diagonal of the cross-section of the square LaB₆ nanowire measured from the TEM image shown in Figure 4a. The effective emission area A was derived to be 6.4 nm^2 after substituting β and ϕ into the y-intercept b of the F–N plot as

$$b = \ln\left(\frac{1.5 \times 10^{-6} A \beta^2}{\phi}\right) + \frac{10.4}{\phi^{1/2}} \quad (2)$$

Although the reason why only a small spot of the relatively large area of the whole tip (about 2000 nm^2) was activated to emit electrons is still unclear, the small emitting area is a desired feature for high-resolution electron optical applications where point electron sources are needed. The emission current density at 800 V was estimated to be about $5 \times 10^5 \text{ A cm}^{-2}$ by dividing the total emission current by the effective emission area. In comparison with the state-of-the-art W/ZrO thermal field emitter working at $1800 \text{ }^\circ\text{C}$ with a 3000 V extraction voltage, the LaB₆ nanowire emitter offers a current density one order of magnitude higher while working at room temperature with an 800 V extraction voltage. The current density of the LaB₆ nanowire emitter was also compared with that of a carbon nanotube field emitter, which was believed to be the most promising field-emitter material of all nanotube/nanowire emitters. Results obtained from a single-walled carbon nanotube bundle emitter under the same experimental configuration show that the current density is at the same order of magnitude as the tested LaB₆ nanowire emitter.^[15] Four other I – V curves were also obtained from the same LaB₆ nanowire emitter with a continuous emitting time duration of 30 min.

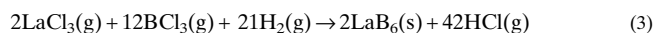
To study the influence of the amorphous boron layer on the field-emission properties of the LaB₆ nanowires, an amorphous boron nanowire about 170 nm in diameter was attached to a tungsten tip and arranged similarly to the LaB₆ nanowire emitter field-emission measurement setup. The

emission current never exceeded 1 nA before the applied voltage rose higher than 800 V, in contrast to the 30 nA stable emission from the LaB₆ nanowire emitter of similar size and under the same applied voltage. This might be due to the high work function of boron (4.5 eV). On the other hand, it also suggests that the field emission from the LaB₆ nanowires should mainly result from the crystalline part of the nanowire rather than the amorphous boron layer. This point of view is also supported by the field-emission data from single-crystalline GdB₆ nanowires with a similar geometry.^[24] With the same amorphous boron layer on a GdB₆ single-crystalline nanowire of work function 1.5 eV, the GdB₆ nanowire emitter has a higher emission current than the LaB₆ nanowire emitter at the same applied voltage. This should not have occurred if it were the amorphous boron layer that played the key role in the field emission.

In summary, straight single-crystalline <001>-oriented LaB₆ nanowires with widths ranging from 15 nm to more than 100 nm have been successfully synthesized by a CVD method. These nanowires are terminated with {001} surfaces and offer a promising structure as point electron sources. Field-emission measurements on a single LaB₆ nanowire showed that a high emission current density of $5 \times 10^5 \text{ A cm}^{-2}$ was achieved at a voltage below 800 V with an effective emission area as small as 6.4 nm^2 . With an even thinner emitter, LaB₆ nanowires offer the prospect to make the best point electron sources as a consequence of the low work function and low dimensionality of this unique material.

Experimental

The synthesis of the LaB₆ nanowires is based on the chemical reaction



The reaction was conducted in a tube furnace operated at $1150 \text{ }^\circ\text{C}$ where BCl₃ gas and LaCl₃ powders were brought together in an atmosphere of hydrogen and nitrogen gases. Single-crystalline nanowires were grown on metal substrates with a good yield and a small amount of amorphous boron impurity, similar to the CVD approaches that have also been used to produce LaB₆ whiskers with diameters over 1 μm [21,22,25–27].

For electron-microscopy observations, the LaB₆ nanowires were first dispersed in ethanol and then collected onto a TEM grid coated with a holey carbon film. A transmission electron microscope (JEM-2010F equipped with a field-emission gun) operated at 200 kV was used in the electron-diffraction and electron-microscopy examinations, as well as for electron energy-loss spectroscopic analysis.

For field-emission measurements, the tungsten wire was used as the cathode and a piece of indium tin oxide (ITO) glass plate was used as the anode. A layer of phosphor was also painted on the ITO glass to enable observation of the electron-emission pattern when field-emission electrons from the cathode reached the anode. The FE measurement was carried out in a high-vacuum chamber at a pressure of 10^{-7} torr.

Received: March 11, 2005

Final version: August 17, 2005

Published online: December 5, 2005

- [1] M. Gesley, L. W. Swanson, *Surf. Sci.* **1984**, *146*, 583.
- [2] L. W. Swanson, M. A. Gesley, P. R. Davis, *Surf. Sci.* **1981**, *107*, 263.
- [3] D. B. Williams, C. B. Carter, *Transmission Electron Microscopy*, Plenum, New York **1996**.
- [4] I. Brodie, C. A. Spindt, in *Advances in Electronics and Electron Physics*, Vol. 83 (Ed: P. W. Hawkes), Academic, San Diego, CA **1992**, Ch. 2.
- [5] R. Shimizu, Y. Kataoka, T. Tanaka, S. Kawai, *Jpn. J. Appl. Phys.* **1975**, *14*, 1089.
- [6] M. Futamoto, S. Hosoki, H. Okano, U. Kawabe, *J. Appl. Phys.* **1977**, *48*, 3541.
- [7] H. Nagata, K. Harada, R. Shimizu, *J. Appl. Phys.* **1990**, *68*, 3614.
- [8] K. Harada, H. Nagata, R. Shimizu, *J. Electron Microsc.* **1991**, *40*, 1.
- [9] S. Zaima, M. Sase, H. Adachi, Y. Shibata, C. Ohshima, T. Tanaka, S. Kawai, *J. Phys. D: Appl. Phys.* **1980**, *13*, L47.
- [10] L. A. Chernozatonskii, Y. V. Gulyaev, Z. J. Kosakovskaja, N. I. Sinitsyn, G. V. Torgashov, Y. F. Zakharchenko, E. A. Fedorov, V. P. Val'chuk, *Chem. Phys. Lett.* **1995**, *233*, 63.
- [11] A. G. Rinzler, J. H. Hafner, P. Nikolaev, L. Lou, S. G. Kim, D. Tomaneck, P. Nordlander, D. T. Colbert, R. E. Smalley, *Science* **1995**, *269*, 1550.
- [12] W. A. D. Heer, A. Chatelain, D. Ugarte, *Science* **1995**, *270*, 1179.
- [13] J. M. Bonard, H. Kind, T. Stockli, L. O. Nilsson, *Solid-State Electron.* **2001**, *45*, 893.
- [14] N. de Jonge, Y. Lamy, K. Schoots, T. H. Oosterkamp, *Nature* **2002**, *420*, 393.
- [15] J. Zhang, J. Tang, G. Yang, Q. Qiu, L.-C. Qin, O. Zhou, *Adv. Mater.* **2004**, *16*, 1219.
- [16] K. W. Wong, X. T. Zhou, C. K. Frederick, H. L. Lai, C. S. Lee, S. T. Lee, *Appl. Phys. Lett.* **1999**, *75*, 2918.
- [17] J. Chen, S. Z. Deng, N. S. Xu, S. Wang, X. Wen, S. Yang, C. Yang, J. Wang, W. Ge, *Appl. Phys. Lett.* **2002**, *80*, 3620.
- [18] Y. Lee, C. Choi, Y. Jang, E. Kim, B. Ju, N. Min, J. Ahn, *Appl. Phys. Lett.* **2002**, *81*, 745.
- [19] Y. B. Li, Y. Bando, D. Golberg, K. Kurashima, *Appl. Phys. Lett.* **2002**, *81*, 5048.
- [20] L.-W. Yin, Y. Bando, Y.-C. Zhu, M.-S. Li, Y.-B. Li, D. Golberg, *Adv. Mater.* **2005**, *17*, 110.
- [21] A. Hagimura, A. Kato, *Nippon Kagaku Kaishi* **1980**, *7*, 1108.
- [22] E. I. Givargizov, L. N. Obolenskaya, *J. Less-Common Met.* **1986**, *117*, 97.
- [23] H. Zhang, Q. Zhang, J. Tang, L.-C. Qin, *J. Am. Chem. Soc.* **2005**, *127*, 8002.
- [24] H. Zhang, Q. Zhang, G. Zhao, J. Tang, O. Zhou, L.-C. Qin, *J. Am. Chem. Soc.* **2005**, *127*, 13120.
- [25] S. Motojima, Y. Takahashi, K. Sugiyama, *J. Cryst. Growth* **1978**, *44*, 106.
- [26] E. I. Givargizov, L. N. Obolenskaya, *J. Cryst. Growth* **1981**, *51*, 190.
- [27] S. S. Kher, J. T. Spencer, *J. Phys. Chem. Solids* **1998**, *59*, 1343.

DOI: 10.1002/adma.200500451

Fluorescence Enhancement by Metal-Core/Silica-Shell Nanoparticles**

By Oleg G. Tovmachenko, Christina Graf,
Dave J. van den Heuvel, Alfons van Blaaderen, and
Hans C. Gerritsen*

The fundamental and applied physics of noble-metal nanoparticles is currently attracting much attention. To a great extent this is due to promising new applications of noble-metal colloidal nanoparticles in fields such as materials science,^[1] biophysics,^[2] molecular electronics, and fluorescence-spectral engineering based on surface-enhancement effects.^[3] In particular the nanoparticles have promising applications as bright fluorescent markers with enhanced photostability in fluorescence microscopy, sensor technology, and microarrays. The enhancement of the fluorescence emission of molecules near a metal surface arises from interactions with surface plasmon (SP) resonances in the metal particles.^[4–6] These interactions may also result in shortening of the excited-state lifetime thus improving the photostability of the dye.^[7]

The optical properties of a fluorescent molecule located near a metal nanoparticle are affected by the near-field electro-dynamical environment.^[4–6] This can cause an enhancement or quenching of the fluorescence depending on the distance between the molecule and the metal surface. In the case of fluorescent molecules located at very short distances from a metal surface, non-radiative energy transfer to SPs in the metal takes place.^[8,9] Electromagnetic-field enhancement due to SPs, however, still occurs at longer distances from the metal core. As a result, there is an optimal fluorescent molecule to metal-core distance for fluorescence enhancement.

Important factors affecting the strength of the fluorescence enhancement are the size and shape of the nanoparticle, the orientation of the dye dipole moments relative to the nanoparticle surface normal, the overlap of the absorption and emission bands of the dye with the plasmon band of the metal, and the radiative decay rate and quantum yield (Q) of the fluorescent molecules.

[*] Prof. H. C. Gerritsen, Dr. O. G. Tovmachenko, Dr. C. Graf,^[†] D. J. van den Heuvel, Prof. A. van Blaaderen
Soft Condensed Matter & Molecular Biophysics Department
Debye Institute, Utrecht University
Princetonplein 1, NL-3584 CC Utrecht (The Netherlands)
E-mail: H.C.Gerritsen@phys.uu.nl

[†] Present address: Institut für Physikalische Chemie, Universität Würzburg, Sanderring 2, 97070 Würzburg, Germany.

[**] This work is part of the research programme of the Stichting voor Fundamenteel Onderzoek der Materie (FOM), financially supported by the Nederlandse Organisatie voor Wetenschappelijk Onderzoek (NWO).